China Geology 6 (2023) 70−84

China Geology

Journal homepage: http://chinageology.cgs.cn
https://www.sciencedirect.com/journal/china-geology

A comparative study of the main factors controlling geohazards induced by 10 strong earthquakes in Western China since the Wenchuan earthquake in 2008

Chao Peng[a], Zhi-qiang Yin[b,*], Xu-jiao Zhang[a], Hai Shao[b], Ming-fei Pang[b, c]

[a] *China University of Geosciences (Beijing)*, *Beijing* 100029, *China*
[b] *China Institute of Geo-Environment Monitoring*, *China Geological Survey*, *Ministry of Natural Resources*, *Beijing* 100081, *China*
[c] *China University of Geosciences*, *Wuhan* 430074, *China*

ARTICLE INFO

Article history:
Received 4 July 2021
Received in revised form 26 November 2021
Accepted 7 December 2021
Available online 25 December 2021

Keywords:
Wenchuan earthquake
Geohazards
Main control factors
Comparative study
Geological disater survey engineering
Western China

ABSTRACT

Determining the main controlling factors of earthquake-triggered geohazards is a prerequisite for studying earthquake geohazards and post-disaster emergency response. By studying these factors, the geomorphic and geological factors controlling the nature, condition, and distribution of earthquake-induced geohazards can be analyzed. Such insights facilitate earthquake disaster prediction and emergency response planning. The authors combined field investigations and spatial data analysis to examine geohazards induced by seismic events, examining ten earthquakes including the Wenchuan, Yushu, Lushan events, to elucidate the main control factors of seismic geohazard. The authors observed that seismic geohazard occurrence is usually affected by many factors, among which active nature of the seismogenic fault, seismic peak ground acceleration (PGA), topographic slope and geomorphic height differences, and distance from the fault zone and river system are the most important. Compared with strike-slip earthquakes, thrust earthquakes induce more high-altitude and high-speed remote landslides, which can cause great harm. Slopes of 0°–40° are prone to secondary seismic geohazards, which are mainly concentrated 0–6 km from the river system. Secondary geohazards are not only related to seismogenic fault but also influenced by the associated faults in the earthquake area. The maximum seismic PGA and secondary seismic geohazard number are positively correlated, and the horizontal and vertical ground motions play leading and promoting roles in secondary geohazard formation, respectively. Through the research, the spatial distribution of seismic geohazards is predicted, providing a basis for the formulation of emergency response plans following disasters.

1. Introduction

The spatial distribution law of secondary geohazards induced by earthquakes and their main controlling factors are important directions in the study of earthquake geohazards. Previous studies have extensively analyzed the factors inducing seismic geohazards (Chen JP et al., 2009; Huang RQ and Li WL, 2009; Han YS et al., 2010; Yin YP and Zhang YS, 2012a; Zhang YS et al., 2013; Song ZC et al., 2018). Huang RQ et al. (2009) studied the impact of faults on geohazards triggered by the Wenchuan earthquake. The authors proposed the geohazards induced by the thrust earthquake showed evidence of "upper/lower wall effects" and fault distance effect and were distributed in a zonal pattern along the fault zone and linearly along the river. Han YS et al. (2010) quantitatively analyzed the effects of elevation, slope, and aspect on the susceptibility of secondary mountain disasters in the Wenchuan section of the Minjiang River valley and determined the topographic conditions most favorable for mountain disasters to occur. Yin YP and Zhang YS (2012a) proposed that the landslide induced by the Wenchuan earthquake was controlled by the seismic fault, where the vertical seismic force in high-seismicity areas was evident, and the landslide had both throwing and air cushioning effects. In addition, some scholars consider the seismic intensity as the primary factor influencing seismic landslides (Zhou BG and Zhang YM, 1994; Ding YH et al., 1999). However, seismic intensity can be determined only

First author: *E-mail address*: pengchao081@163.com (Chao Peng).

* Corresponding author: *E-mail address*: yinzhiqiang@mail.cgs.gov.cn (Zhi-qiang Yin).

Literary editor: Xi-jie Chen
doi:10.31035/cg2022009
2096-5192/© 2023 China Geology Editorial Office.

subjectively by investigating the damage caused by an earthquake to people, man-made structures, and the natural environment, often considerably after the seismic event. Moreover, seismic geohazards are one factor used to determine seismic intensity, giving rise to an issue of mutual reference. Generally, high-intensity areas are generally coincident with the concentrated areas of geohazards; however, in some areas, using only intensity as the basis for emergency response assessment of post-earthquake geohazards deviates substantially from the actual situation.

Among the many influencing factors of seismic geohazards, the nature and fracture mode of the active fault zone is important (Wang DP et al., 2013; Zhang YS et al., 2013); however, whether it plays a dominant role is an unresolved question. Furthermore, the occurrence of geohazards is influenced by peak ground acceleration (PGA), topographic slope, terrain elevation, and distance from the seismogenic fault and river system; however, it is unclear which factors dominate. Notably, analyzing these factors to determine how to prioritize areas for emergency rescue response following an earthquake disaster is key.

Considering ten representative earthquake-induced geohazards in China 's western mountains since 2008, the authors conducted a comparative study on the various geohazards arising in the earthquake zone. The authors attempted to analyze the main factors that induce geohazards in this region, which are subject to severe recurrent earthquakes, to facilitate the development of geohazard reference information to assist emergency rescue plans.

2. Geological settings

China is located between the Pacific Rim Seismic Belt and the Asia–Europe Seismic Belt. Compressed by the Pacific Plate, Indian Plate, and Philippine Sea Plate, China has developed tectonic fault zones and is prone to earthquakes. The ten earthquakes investigated in this study are distributed across western China (Fig. 1). This area is the transition zone from the first to the second step of Chinese mainland topography, and it is the most active area of neotectonic movement. It experiences rapid crustal uplift, strong plate compression, and frequent earthquakes. Due to the influence of the rapid uplift of the Qinghai–Tibet Plateau, many active fault zones and extreme geomorphological height differences have been formed in the western region. Since 2008, many large-scale earthquake events have occurred in the mountainous areas of western China. These earthquakes have not only caused many casualties and property losses but also triggered tens of thousands of landslides, collapses, and other geohazards, forming a significant post-earthquake secondary

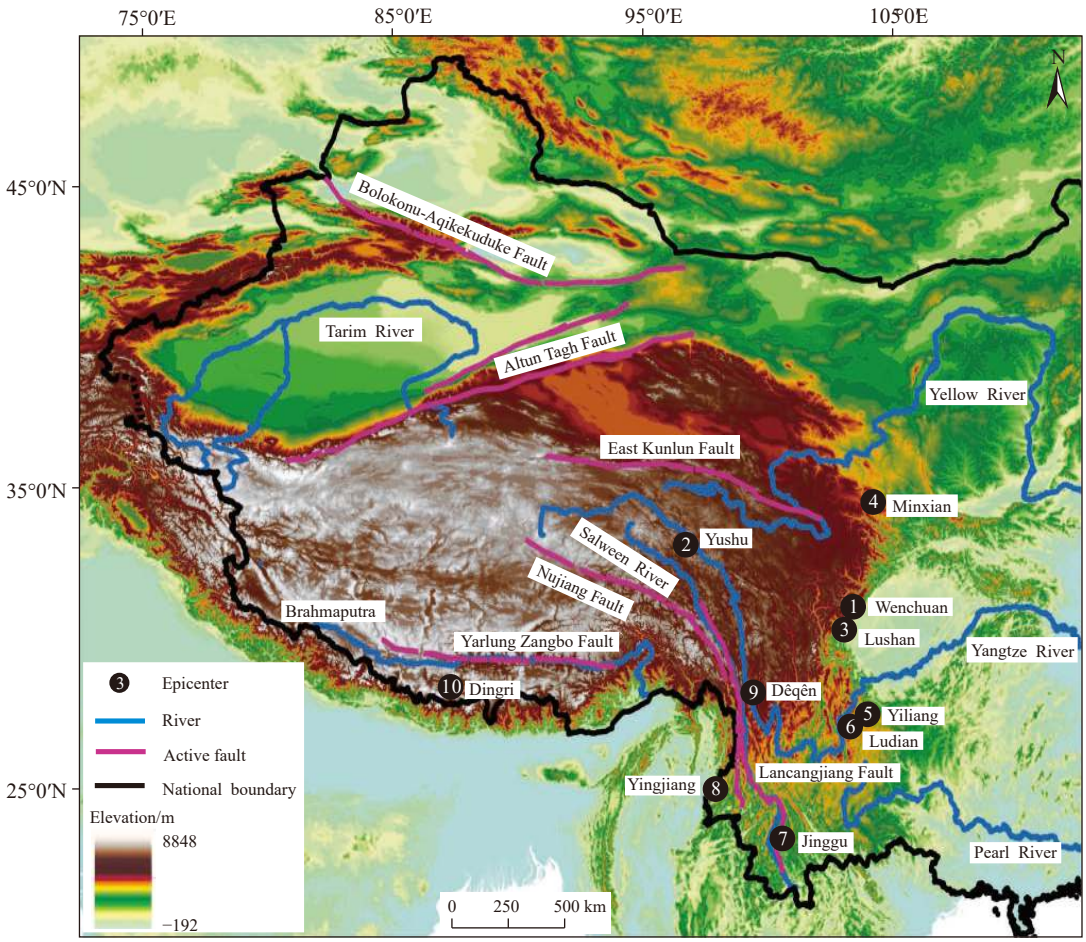

Fig. 1. Distribution map of 10 strong earthquakes in western China (China basemap after China National Bureau of Surveying and Mapping Geographical Information; 1–10 are earthquake numbers, as shown in Tables 1–2) .

disaster chain effect (Table 1). For example, the Wenchuan M_S 8.0 earthquake that occurred on the Longmenshan Fault zone on May 12, 2008, triggered over 56000 geohazards (Dai FC et al., 2011; Tang C et al., 2011); it also induced many high-speed remote giant landslides and clastic flow landslides (Yin YP et al., 2011, 2012b; Wang YF et al., 2012; Lan J and Chen XL, 2020) that formed 33 barrier lakes (Cui P et al., 2009), and approximately 10000 people died or went missing due to these secondary geohazards. The M_S 5.7 and M_S 5.6 earthquake in Yiliang on September 7, 2012, triggered 259 landslides, 189 collapses, and rock-rolling disasters, triggering a collapse-landslide-debris flow disaster chain event (Wang DP et al., 2013); this caused the landslide at Tiantou primary school in which 19 people were killed, and the slide body blocked the river to form a dammed lake. The M_S 6.5 earthquake in Ludian on August 3, 2014, triggered over 1700 secondary geohazards and formed the Ganjiazhai landslide with a volume of 8.4×10^6 m^3, which caused the village to be buried and destroyed with 55 casualties. It also formed a 120 m high and approximately 12×10^6 m^3 large damming body, threatening the safety of over 30000 people downstream (Xu YQ et al., 2016; Yin ZQ et al., 2016; Yang XY and Yao YH, 2018; Wu WY et al., 2020).

3. Materials and methods

Firstly, ten collected seismogenic information and geospatial data about the distribution of secondary geohazards arising from the ten earthquakes from authorities and conducted field investigations on some typical seismic area. The coordinate information of geohazard points and disaster investigation reports were gathered from the post-disaster emergency investigation departments in each earthquake area. Information on distribution of the seismogenic fault zone (s) and seismic intensity were collated from the China Earthquake Administration. The seismic PGA data are provided by China Strong Motion Network Centre at Institute of Engineering Mechanics, China Earthquake Administration. The field investigation method is based on the *Post-earthquake field works —part 3: code for field survey (GB/T18208.3-2011)* and *Technical requirement for geohazard survey (1:50000) (DD2019-08)*. Then, using the ArcGIS10.3 platform, the geohazard locations, seismic, geological, and geomorphic information are projected onto the DEM base map of each earthquake area. From this, a diagram depicting the relationship between geohazard location and potential inducing factors in the ten earthquake areas was generated (Figs. 2–7). Finally, the data of topographic slope, geomorphological elevation, and distance from geohazard locations to faults and water systems in each earthquake area are extracted to examine the statistical relationship between geohazard location and seismic, geomorphic and geological factors. Through comparative analysis, this study investigates the similarities and differences among the inducing factors of secondary geohazards in different earthquake areas, to determine the main controlling factors of seismic geohazards.

4. Result and analysis

The formation and distribution of seismic geohazards are usually affected by a variety of controlling factors. Due to the

Table 1. Comparison of characteristics of ten strong earthquakes in western China since 2008.

No.	Earthquake name	M_S	Focal depth/km	Intensity	Epicenter	Seismic fault/type	Average slope/°	Fatalities	Number of geohazards
1	Wenchuan earthquake	8.0	14	Ⅵ-Ⅺ	Yingxiu	Beichuan-Yingxiu Fault/ Thrust predominates, with a dextral strike-slip component	20.3	87652	56000
2	Yushu earthquake	7.1	14	Ⅴ-Ⅸ	Longbao	Ganzi-Yushu Fault / Sinistral strike-slip	18.6	2220	282
3	Lushan earthquake	7.0	13	Ⅵ-Ⅸ	Longmen	Dachuan-Shuangshi Fault/ Blind thrust fault	19.0	196	3000
4	Minxian–Zhangxian earthquake	6.6	20	Ⅵ-Ⅷ	Minxian–Zhangxian junction	Lintan-Dangchang Fault/ Strike-slip predominates and has a thrust component	19.0	95	328
5	Yiliang earthquake	5.7+5.6	14	Ⅵ-Ⅷ	Luozehe	Zhaotong-Ludian Fault/ Strike-slip type with a small amount of thrust	17.9	81	366
6	Ludian earthquake	6.5	12	Ⅵ-Ⅸ	Longtoushan	Baogunao-Xiaohe Fault/ Sinistral strike-slip	19.5	729	1707
7	Jinggu earthquake	6.6	5	Ⅵ-Ⅷ	Yongping	Puwen Fault/ Strike-slip type	19.1	1	109
8	Yingjiang earthquake	6.1	12	Ⅵ-Ⅷ	Kachang	Sudian Fault/ Dextral strike-slip	15.1	0	172
9	Dêqên earthquake	5.9	10	Ⅵ-Ⅷ	Dêqên–Derong junction	Dêqên-Zhongdian Fault/ Normal fault predominates, with a sinistral strike-slip component	27.7	3	86
10	Dingri earthquake	5.9	20	Ⅵ-Ⅸ	Dingri	A low-angle thrust fault zone along the south main boundary of the Himalayan orogenic belt	19.8	27	198

Note: Earthquake magnitude difference of 1 level, the energy released by the difference of 31.6 times.

variety of factors influence geohazard formation, including earthquake magnitude, PGA, fault activity, topography, and geomorphology of the earthquake area, and the effects of post-earthquake rainfall, there is a wide variation in the number, scale and degree of damage between different geohazard events. All ten earthquakes analyzed in this study are tectonic earthquakes caused by fault activity, and the types of geological disasters induced are similar, primarily including landslides, collapse, debris flows, rolling rocks, dammed lakes, and sand liquefaction (Table 2).

Wenchuan, in northwestern Sichuan Province, is in the transition zone between the first and second steps of China's landform, with the terrain descending from NW to SE. Its landform types include plateaus, mountains, and plains with large height differences (7035 m), steep topographic slopes (average 20.3°), and complex geological structures (Figs. 2a, b). The regional structure is in the Longmenshan Fault zone, which is highly active on the eastern margin of the Qinghai–Tibet Plateau (Liu CZ et al., 2016). The seismic area is mainly controlled by the Beichuan–Yingxiu Fault (F_1), Guanxian–Jiangyou Fault (F_2), and Wenchuan–Maoxian Fault (F_3); the river systems include the Minjiang, Bailong, Peijiang, and Jialing rivers. The seismogenic fault is the Beichuan–Yingxiu Fault (F_1), which has mainly thrust and some dextral strike-slip component. The M_S 8.0 Wenchuan earthquake on May 12, 2008, induced geohazards that were mainly concentrated in the hanging wall of the fault zone (NW), accounting for approximately 80% of the total geohazards, and were mainly in the Ⅷ–Ⅺ intensity zone, of which the extremely large, high-speed remote landslides events were mainly inside the Ⅸ–Ⅺ intensity zone. Most of the disaster points (95.1%) were concentrated at elevations of 500–3500 m (Fig. 2a), and 61.2% were distributed within the 20°–40° slope range (Fig. 2b). The average distances from the disaster locations to the seismogenic fault (F_1) and river system were 28.7 km and 3.6 km, respectively.

Lushan is in the northwest of Sichuan Province, in the transitional zone between the western margin of the Sichuan Basin and the Qinghai–Tibet Plateau and the southern end of the Longmenshan Fault zone. The geological structure is complex, the topography is high in the west and low in the east, whereas the topographic slope gradually decreases heading east (Figs. 2a, b). The main river systems include the Qingyi, Yuxi, and Danan rivers. The main seismogenic fault is the Dachuan–Shuangshi Fault (F_4), which is thrust fault. The M_S 7.0 Lushan earthquake on April 20, 2013, induced geohazards mainly concentrated in the Ⅷ–Ⅹ intensity zone. Many of the disaster points (83%) were concentrated at elevations of 500–1500 m (Fig. 2a), and 94.4% were distributed between 0–40° slope (Fig. 2b). The average distances from the disaster points to the seismogenic fault (F_4) were 9.4 km and 2.0 km, respectively.

The Minxian-Zhangxian earthquake occurred in the southeastern part of Gansu Province, in the middle of China's south–north seismic belt and at the junction of the northeastern edge of the Qinghai–Tibet Plateau and southeastern Gansu (Xiao WB et al., 2020), which is a loess landform. The overall terrain is high in the south and low in the north, with an average elevation of 2500 m and a steep topographic slope in the southwest and gentle in the northeast (Figs. 2a, b). The main faults are the Lintan–Dangchang Fault (F_5), the north margin fault of West Qinling (F_6), the southern Guanggaishan–Dieshan Fault (F_7), and the Bailongjiang Fault (F_8); the main river systems include the Taohe, Weihe, and Bailong rivers. The main seismogenic fault is the Lintan–Dangchang Fault (F_5), comprising mainly strike-slip and some

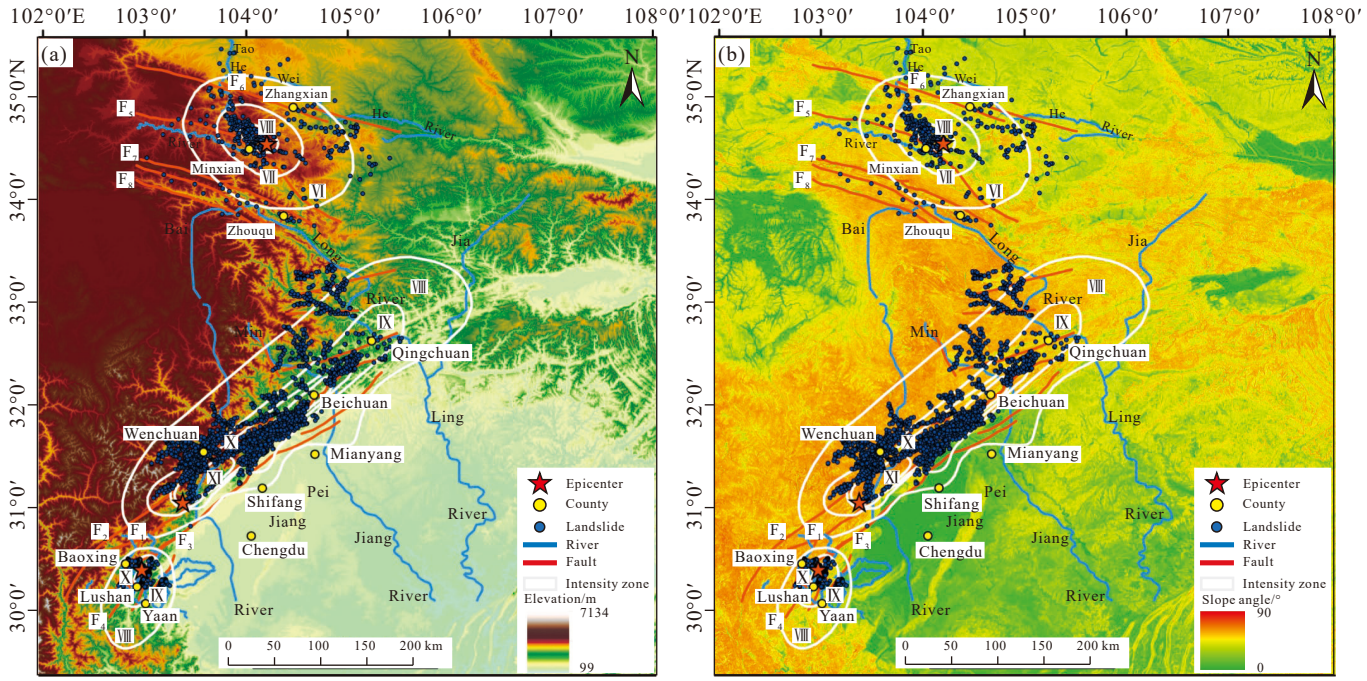

Fig. 2. Relationship between the distribution of secondary geohazards and elevation (a) and slope (b) in Wenchuan, Lushan and Minxian-Zhangxian earthquake.

thrust component. The M_S 6.6 Minxian–Zhangxian earthquake on July 22, 2013, induced geohazards were mainly concentrated in the Ⅵ–Ⅷ intensity zone. Many of the disaster points (83.6%) were concentrated at elevations of 2000–3000 m (Fig. 2a), and 92.7% were distributed between 0°–30° slope (Fig. 2b). The average distances from the disaster points to the seismogenic fault (F_5) and river system were 27.2 km and 3.5 km, respectively.

Yushu is in the southern part of Qinghai Province. Its overall topography is high in the northwest and middle, low in

Table 2. Comparison of geohazards induced by ten strong earthquakes in western China since 2008.

No.	Name	Geohazards type	Geohazard characteristics	Harm degree	Typical geohazards	Main control factors
1	Wenchuan earthquake	Collapse Landslide Debris flow Rolling stones Dammed lake Sand liquefaction	Geological disasters are numerous and large in volume. Massive high-speed remote landslides, and the barrier lake has great potential danger.	Geological disasters directly caused over 10×10^3 deaths, and only the landslide in Beichuan west caused over 1600 deaths and disappearances. Direct economic losses exceeding RMB 800×10^9.	The Daguangbao landslide with a volume of 1159×10^6 m^3 was induced, which is the largest landslide ever recorded in China. The Donghekou landslide, with a volume of over 100×10^6 m^3, buried 7 villages and killed over 780 people (Cui SH et al., 2020).	(1) Active fault (2) Topographic slope (3) Geomorphic height difference (4) PGA
2	Yushu earthquake	Collapse Landslide Debris flow Unstable slope Surface rupture Sand liquefaction	Geohazards number increased significantly; spatial distribution was controlled by faults. The low-soil and eluvial layer landslide is more prominent, and the effect of geohazards-chain is evident.	Yushu County is the most densely distributed and the most unsafe. The geological disaster in Jiegu was seven times that before the earthquake, resulting in 8 deaths, 14 injuries, and direct economic losses of RMB 0.6×10^6 yuan.	There were no large-scale geohazards (hidden spots) after the earthquake, and the main types of disasters were debris flow disaster chain, mostly distributed on the right bank of Tongtianhe River in the county and urban area.	(1) Active fault (2) Topographic slope (3) Geomorphic height difference (4) River system
3	Lushan earthquake	Collapse Landslide Debris flow Rolling stones Dammed lake	Smaller monomer scale, mainly shallow surface collapses and landslides. Formation mechanisms including: tensile crack–collapse–collision–scraper–debris flow, vibration– throwing, etc.	Secondary disasters did not cause death, only causing partial property losses.	Induced the Gangoutou landslide with a volume of 2480×10^3 m^3 and a large debris flow ditch-Lengmugou debris flow.	(1) Active fault (2) PGA (3) Geomorphic height difference (4) River system
4	Minxian-Zhangxian earthquake	Collapse Landslide Debris flow Rolling stones	The total number of geohazards after the earthquake rose by 16%, and it was mainly distributed in the area from Lalu Village to Baozi Village, mainly loess collapses and landslides.	The earthquake-induced loess landslide directly killed 14 people and damaged over 100 houses.	The largest and most harmful landslides in Wamuchi $1^{\#}$ and $2^{\#}$ which directly caused 12 deaths. Another typical one is the landslide in Baozi Village, with a volume of approximately 1×10^6 m^3, causing two deaths.	(1) Active fault (2) Stratigraphic lithology (3) Aftershocks (4) Rainfall
5	Yiliang earthquake	Collapse Landslide Debris flow Rolling stones	The geohazards are numerous, widely distributed and of different sizes, and mainly occur along the slope weathering unloading zone or residual slope layer. Yiliang County is the most densely distributed.	The rolling stones induced by the earthquake killed and injured many people and led to traffic blockage and house damage. A landslide in Youfang Village one month after the earthquake killed 19 people (Wang DP et al., 2013).	The main disaster point is the collapse of Shitouzhai, its volume is approximately 3500 m^3 and the height difference is approximately 200 m. It is caused by the joints and fissures of limestone in the Lower Permian Qixia Maokou Formation.	(1) Active fault (2) Rainfall (3) Geomorphic height difference (4) River system
6	Ludian earthquake	Collapse Landslide Debris flow Ground collapse Ground fissure Unstable slope	Geohazards are numerous, complete in type, and widely distributed. They are mainly distributed densely along the Baogunao–Xiaohe Fault and the Zhaotong–Ludian Fault and distributed along the canyon in a zonal pattern. The landslides have the characteristics of "dry landslide" (Yin ZQ et al., 2017).	There were 1770 geohazards, of which 750 were added, accounting for 42%. The number of disaster points was relatively large, and most were high-altitude remote landslides. The disaster resulted in 87 deaths, 40364 households with 181857 people affected, and approximately RMB 4.396 $\times10^9$ of assets under threat (Wang Y et al., 2016).	The collapse and landslide of Hongshiyan formed the Niulanjiang dammed lake with a volume of approximately 120×10^6 m^3, threatening the lives and property of over 30×10^3 people in ten villages downstream. Ganjiazhai landslide and Wangjiapo landslide killed 18 people, 65 people were missing, and 48 houses were buried or damaged.	(1) Active fault (2) Topographic slope (3) Geomorphic height difference (4) River system (5) PGA

Table 2. (*Continued*)

No.	Name	Geohazards type	Geohazard characteristics	Harm degree	Typical geohazards	Main control factors
7	Jinggu earthquake	Collapse Landslide Ground fissure Rolling stones Sand liquefaction	The proportion of new disaster points is small, and the main types of geohazards are shallow small landslides and collapses. The disaster sites are mainly distributed in Jinggu County and are mainly landslides.	Due to the small topographic relief in the earthquake area, the earthquake amplification effect is not evident, and the vegetation coverage rate is high, the population density is small, and therefore, the damage caused by the disaster is small, with no casualties.	None	(1) Active fault (2) River system (3) Human activities
8	Yingjiang earthquake	Collapse Landslide Debris flow Unstable slope	Earthquake-induced 40 new geological disaster sites, mainly distributed in Kachang Town and Mengnong township; the main types of disasters are landslides and unstable slopes, accounting for 72.5%.	Seismic-induced geological disasters are small in number, low in density and small in scale, causing only part of the mountain to crack and causing no casualties.	None	(1) Active fault (2) Geomorphic height difference (3) River system (4) Human activities
9	Dêqên earthquake	Collapse Landslide Debris flow Unstable slope	The earthquake triggered 72 geological disaster sites, among which 42 were newly added, accounting for 58.3%, mainly collapsing, followed by landslides and unstable slopes, and fewer debris flow.	The earthquake-induced landslides and collapses in many mountains, interrupted communications, electricity, and water and damaged many infrastructures such as bridges, farmland, and water conservancy. The collapse of rocks caused one death and a direct economic loss of RMB 1455×10^6 (Yang J et al., 2015).	None	(1) Active fault (2) Topographic slope (3) Geomorphic height difference (4) River system
10	Dingri earthquake	Collapse Landslide Debris flow Subgrade settlement Ground fissure	Geohazards have many types, large quantity and small single scale, and are generally distributed toward NWW. Landslides show evident characteristics of "dry landslide" (Wu XN et al., 2017).	The earthquake resulted in 26 deaths, 3 missing, 856 injured, approximately 300×10^3 people affected. Over 80% of the houses in the earthquake area were damaged to varying degrees, and the direct economic loss reached RMB 33.294×10^9.	The Resuoqiao landslide in Chongse Village, Jilong Town, with an area of 1410×10^3 m^2 and a volume of approximately 2.7×10^6 m^3, slid into the Jilongzangbu River, blocking the road from Jilong Town to the port and affecting the safety of the port.	(1) Active fault (2) Topographic slope (3) Geomorphic height difference (4) River system

the southeast and in the east, dominated by alpine valleys and mountain landforms, with a gentle topographic slope (average 18.6°) (Figs. 3a, b). The main faults in the region are the Ganzi–Yushu Fault (F_1), Gicuonan–Batang Fault (F_2), and Dabeitong–Xiaosumang Fault (F_3), and the main river systems include the Tongtian, Ziqu, and Zhaqu rivers. The main seismogenic fault is the Ganzi–Yushu Fault (F_1) with mainly sinistral strike-slip motion. The M_S 7.1 Yushu earthquake on April 14, 2010, induced geohazards mainly concentrated in the Ⅶ–Ⅷ intensity zone, accounting for approximately 73.5% of the total. Most of the disaster points (94.2%) were concentrated at approximately 3500–4500 m (Fig. 3a), and 92.8% were distributed within the 0°–40° slope range (Fig. 3b). The average distances from the disaster points to the seismogenic fault (F_1) and river system were 21.1 km and 2.3 km, respectively.

Yiliang is on the slope belt on the northeastern edge of the Yunnan–Guizhou Plateau, which belongs to the northeastern Yunnan folded belt of the Yangtze–Quasi platform, with high mountains and deep valleys. Yiliang is the landform of medium mountains and valleys, with the overall terrain being high in the SW and low in the NE, whereas the topographic slope is high in NE and low in SW (Figs. 4a, b). The area mainly develops the NW-trending Zhaotong–Ludian Fault (F_1), Shimen Fault (F_2), and Wulianfeng Fault (F_3), and the main river systems include the Niujie, Hengjiang, and Luoze rivers. The seismogenic fault is the Zhaotong–Ludian Fault (F_1), which comprises mainly strike-slip and some thrust component. The M_S 5.7 Yiliang earthquake on September 7, 2012, induced geohazards were mainly concentrated in the Ⅶ–Ⅷ intensity zone, accounting for approximately 90% of the total. Many of the disaster points (88.3%) were concentrated at 1000–2000 m (Fig. 4a), and 68.8% were distributed between the 10°–30° slope (Fig. 4b). The average distances from the disaster points to the seismogenic fault (F_1) and river system were 10.5 km and 1.3 km, respectively.

Ludian area is in northeastern Yunnan Province, which belongs to the Wumeng Mountain area of the

Yunnan–Guizhou Plateau. It is an alpine canyon with large geomorphological height difference (3842 m), steep topographic slope (average 19.5°), high regional ground stress, frequent seismicity, brittle rocks, and complex geological conditions (Figs. 4a, b). The Baogunao–Xiaohe Fault (F_4), the Zhaotong–Ludian Fault (F_1), and the Wulianfeng Fault (F_5) are mainly developed in this area, and the main river systems include the Niulan, Sayu, and Heishui rivers. The main seismogenic fault is the Baogunao–Xiaohe Fault (F_4), and its activity property is a sinistral strike-slip. The M_S 6.5 Ludian earthquake on August 3, 2014, induced geohazards mainly concentrated in the Ⅶ–Ⅸ intensity zone, accounting for approximately 90% of the total. Many of the disaster points (80.8%) were concentrated at 1500–2500 m (Fig. 4a), and 94% were distributed between the 0°–40° slope (Fig. 4b). The average distances from the disaster points to the seismogenic fault (F_4) and river system were 8.1 km and 4.5 km, respectively.

The Jinggu earthquake zone is in the southwestern part of Yunnan Province, at the southern end of the Hengduan Mountains. It includes complex terrain, numerous mountains, and large vertical topographic variation. The landforms are mainly cut mountains with a geomorphic elevation difference of 3107 m and an average topographic slope is 19.1° (Figs. 5a, b). The Puwen Fault (F_1), the Lancangjiang Fault (F_2), and the Jinggu Fault (F_3) are mainly developed in the area; the main river systems include the Lancang, Chengyuan, and Nanting rivers. The main seismogenic fault is the strike-slip Puwen Fault (F_1). The M_S 6.6 Jinggu earthquake on October 7, 2014, induced geohazards were mainly concentrated in the NW direction and Ⅵ intensity zone. Many of the disaster points (85%) were concentrated at the height of 1000–2000 m (Fig. 5a), and 98.9% were distributed between the 0°–30° slope (Fig. 5b). The average distances from the disaster points to the seismogenic fault (F_1) and river system were 35.9 km and 4.2 km, respectively.

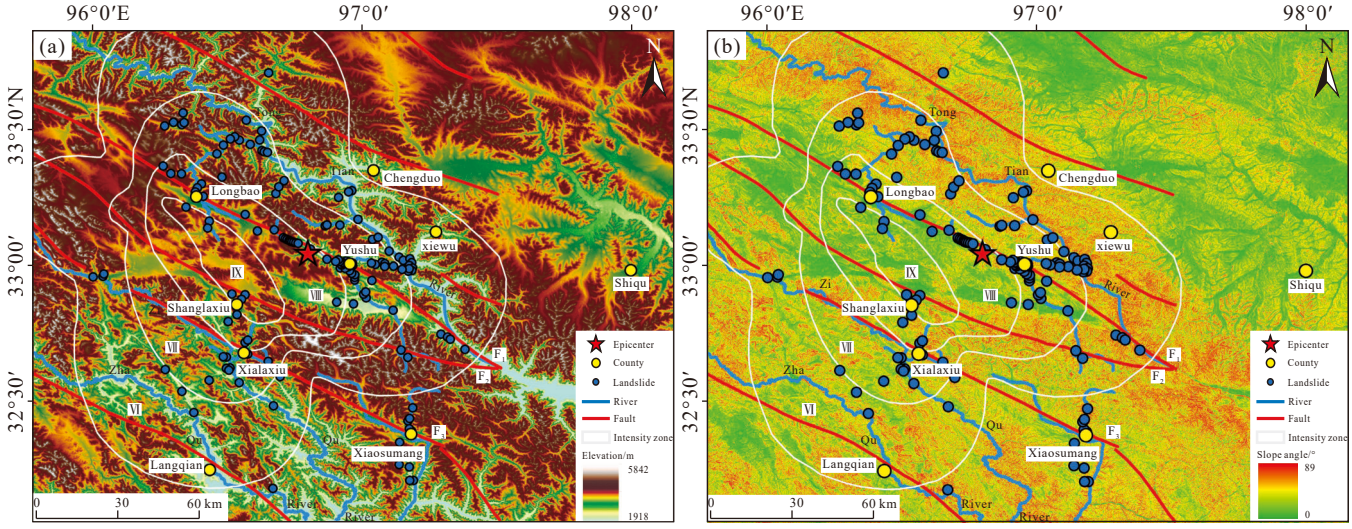

Fig. 3. Relationship between the distribution of secondary geohazards and elevation (a) and slope (b) in Yushu earthquake.

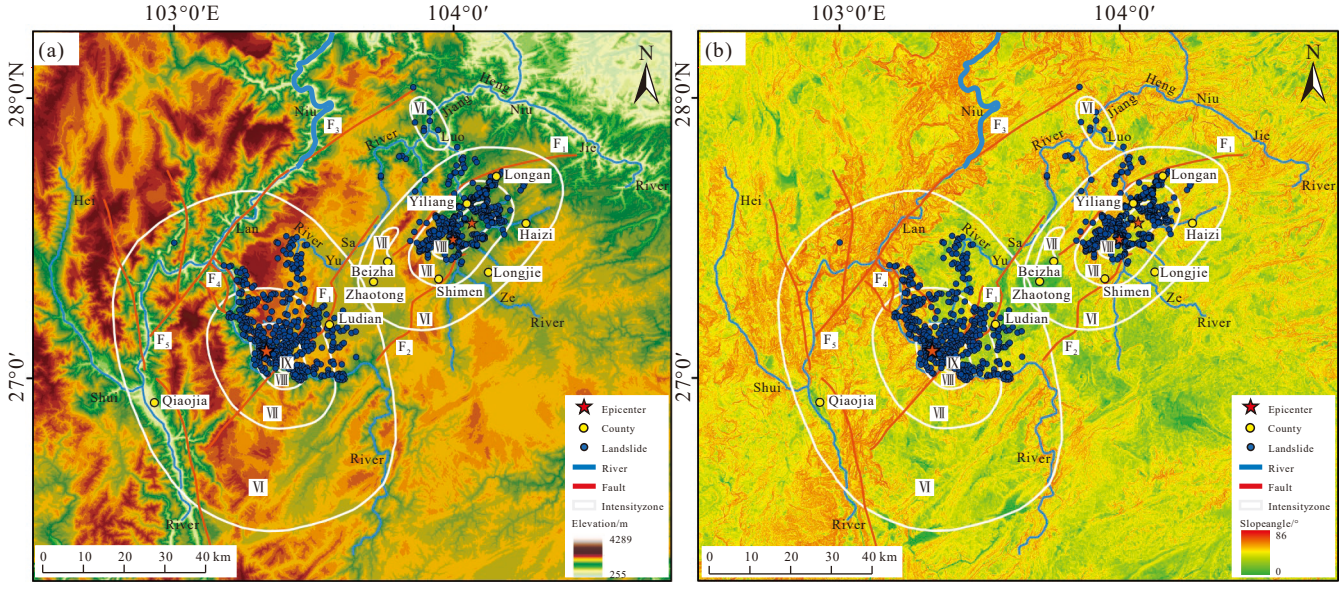

Fig. 4. Relationship between the distribution of secondary geohazards and elevation (a) and slope (b) in Yiliang and Ludian earthquake.

Yingjiang is in the northwestern part of Dehong Prefecture, Yunnan Province. Due to frequent neotectonic movements and intermittent upliftment, the landform is characterized by multiple layers. The terrain height gradually decreases from NE to SW with a gentle topography and an average slope of 15.1° (Figs. 5a,b). The area includes the SN-trending Sudian Fault (F_4) and the NW-trending Dayingjiang Fault (F_5), and the main river systems include the Daying, Mengga, and Nandi rivers. The main seismogenic fault is the dextral strike-slip Sudian Fault (F_4). The M_S 6.1 Yingjiang earthquake on May 30, 2014, induced geohazards mainly concentrated in the Ⅵ–Ⅷ intensity zone. Many of the disaster points (77.4%) were concentrated between 1000–2000 m (Fig. 5a), and 94.1% were distributed between the 0°–30° slope (Fig. 5b). The average distances from the disaster points to the seismogenic fault (F_4) and river system were 16.8 km and 2.7 km, respectively.

Dêqên is in the northwest of Yunnan Province, in the longitudinal valley area of the Hengduan Mountains on the southeast edge of the Qinghai–Tibet Plateau. It is characterized by high altitude (6704 m), large geomorphological height difference (5362 m) and steep topographic slopes (average 27.7°) (Figs. 6a, b). The main active faults include the Dêqên–Zhongdian Fault (F_1), Jinshajiang Fault (F_2), and Lancangjiang Fault (F_3); the Lancang River and Jinsha River run through the whole region from north to south. The main seismogenic fault is the Dêqên–Zhongdian Fault (F_1), which is a normal fault with a sinistral strike-slip component. The M_S 5.9 Dêqên earthquake on August 31, 2013, induced geohazards mainly concentrated in the Ⅵ–Ⅶ intensity zone. Most of the disaster points (94%) were concentrated at 2000–3500 m (Fig. 6a), and 76.7% were distributed between the 10°–40° slope (Fig. 6b). The average distances from the disaster points to the seismogenic fault (F_1) and river system were 12.0 km and 2.5 km, respectively.

Dingri is in the southwest of the Tibet Autonomous Region, where China and Nepal border each other. The epicenter of this earthquake was only 256 km away from the epicenter of an M_S 8.1 earthquake in Nepal. The earthquake zone in Dingri is on the southern slope of the Himalayas, with an average elevation of > 4000 m; it has high and steep topography, complex strata, and lithology, frequent tectonic

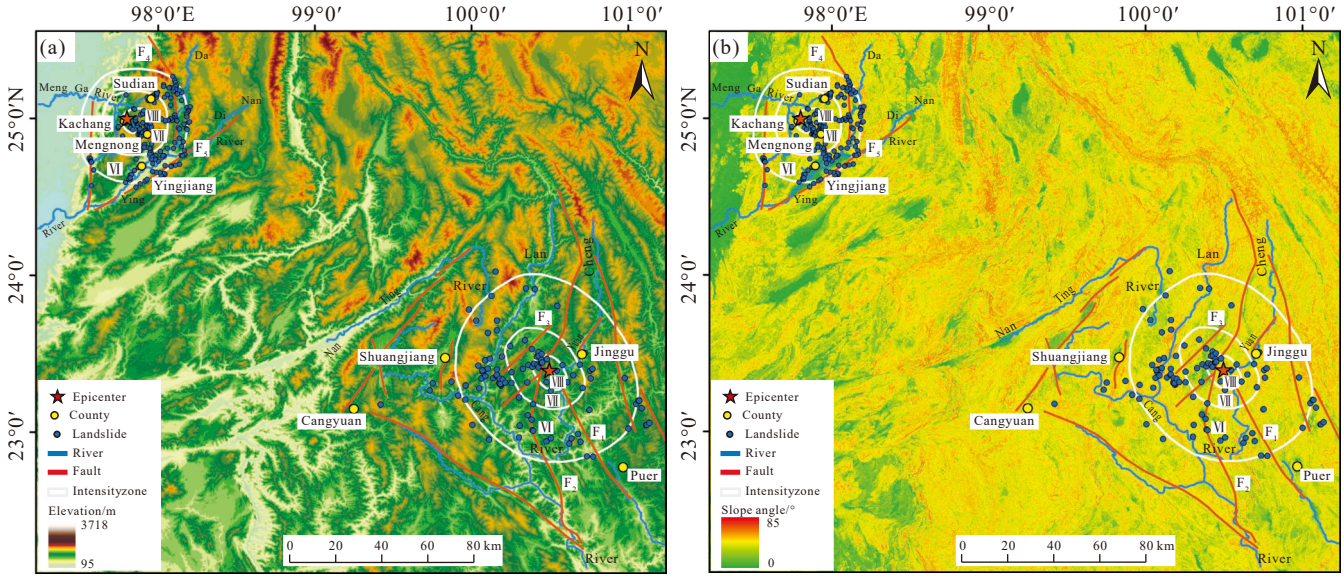

Fig. 5. Relationship between the distribution of secondary geohazards and elevation (a) and slope (b) in Jinggu and Yingjiang earthquake.

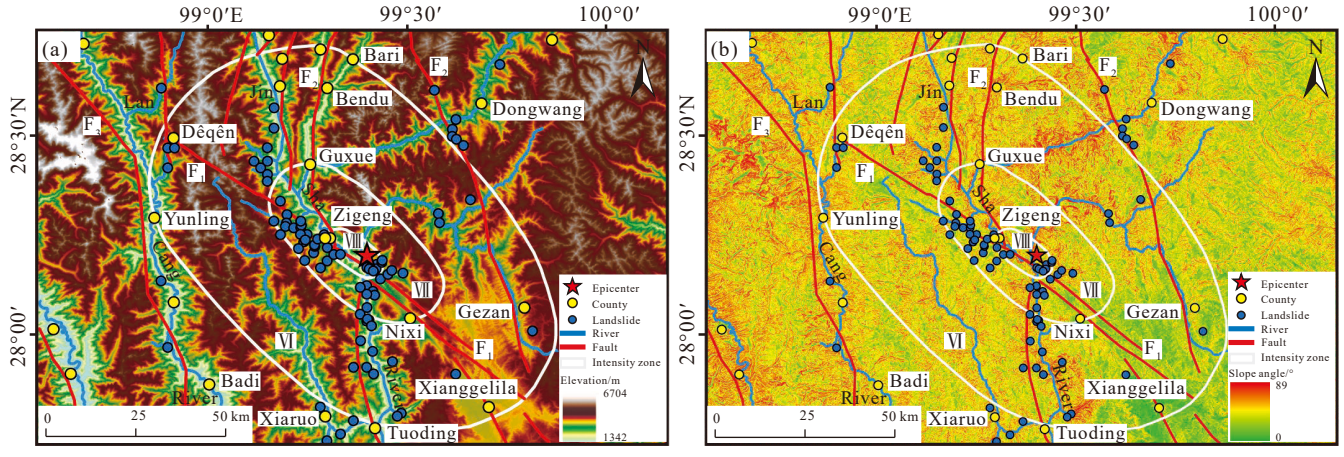

Fig. 6. Relationship between the distribution of secondary geohazards and elevation (a) and slope (b) in Dêqên earthquake.

activity, and dense fault zones (Figs. 7a, b). The river system is dense, mainly including the Duoxiongzangbu, Maquan, and Pengqu rivers. The main seismogenic fault is a low-angle thrust fault zone along the south main boundary of the Himalayan orogenic belt. The M_S 5.9 Dingri earthquake on April 25, 2015, induced geohazards mainly concentrated in the Ⅵ–Ⅷ intensity zone, and 72.1% of the disaster points are concentrated at elevations of 3500–5500 m (Fig. 7a), and 82.2% were distributed between 0°–40° slope (Fig. 7b). The average distances from the disaster points to the fault zone and river system were 2.0 km and 2.2 km, respectively.

5. Discussion

Among the geohazard-inducing factors, earthquakes and rainfall, or their coupling, often trigger secondary disasters. Seismic geohazards mainly occur in the areas of active faults and strong weathering, whereas the geohazards induced by rainfall mainly occur in areas of residual alluvium, soil–rock interfaces with a sliding surface, and interfaces between stratified rock and bedrock (Yuan RM et al., 2010; Chen XL et al., 2011). The two types of disaster mechanisms are evidently different, and therefore, there are significant differences in the main controlling factors between earthquake-induced and rainfall-induced geological hazards.

According to the previous studies, the main controlling factors of seismic geohazards are the active nature of seismogenic fault, seismic PGA, topographic slope, and geomorphological height difference, and distance from fault zones and river systems.

5.1. Active nature of the fault

Earthquakes are usually controlled by fault activity, according to the nature of the seismogenic structures and mechanism of fault movement; the nature of the fault activity can be divided into thrust and strike-slip types. The post-earthquake disaster effects caused by the two different seismic motions are significantly different (Xu C et al., 2012); these directly affect the number, scale, and distribution characteristics of secondary disaster points. In addition, the secondary geohazards induced by thrust-type faults have a significant upper/lower wall effect, because the upper wall of the thrust fault, as the active plate of the fault activity, has a PGA much higher than the lower wall, and the attenuation rate of PGA is far less than that of the lower wall (Li XJ et al., 2008). Therefore, the fault's upper wall releases more energy, experiences longer duration events, and causes more damage throughout the earthquake process.

This study shows thrust faults are more destructive than strike-slip faults, and the secondary geohazards induced are more numerous, larger in scale, and have significant upper/lower wall effects. For example, in the 2008 Wenchuan earthquake, the Beichuan-Yingxiu Fault (F_1) predominantly experienced thrust activity with a dextral strike-slip component, and the secondary geohazards induced by it had significant upper/lower wall effect. The distribution, quantity, scale, and density of disaster points in the upper wall of the fault are evidently higher than those in the lower side (Fig. 8), and they are mainly distributed within 10 km from the upper wall of the seismogenic fault. In addition, most of the extra-large landslides occur in the upper part of the fault, such as the Daguangbao landslide in Anxian, and the Wenjiagou landslide in Mianzhu. In contrast, the secondary geohazards induced by strike-slip faults, such as those arising from the Yushu, Minxian-Zhangxian, and Yiliang earthquakes, have no conspicuous upper/lower effect, and the number, scale, and destructibility of secondary geohazards are far less than that of the Wenchuan earthquake. Therefore, the active nature of seismogenic faults and surface rupture patterns should be considered first in the emergency response of post-earthquake geohazards.

5.2. Seismic peak ground acceleration (PGA)

The earthquakes influence geohazards mainly because the reciprocating seismic motion destroys the balance of slopes and leads to instability; the most significant influence is the seismic PGA. Wang XY et al. 2010, Wang XY (2010) and Wang XY and Wang DW et al. (2011) through the study of the relationship between PGA and secondary geohazards in the Wenchuan earthquake, considered that the peak acceleration of 0.2 g was the dividing line of whether a landslide disaster is serious, and the range of landslide disasters triggered by peak ground velocity was 0.5–1.5 m/s. With the increase in the number of earthquake monitoring stations and the improvement of the monitoring network, PGA data can be obtained immediately after the earthquake,

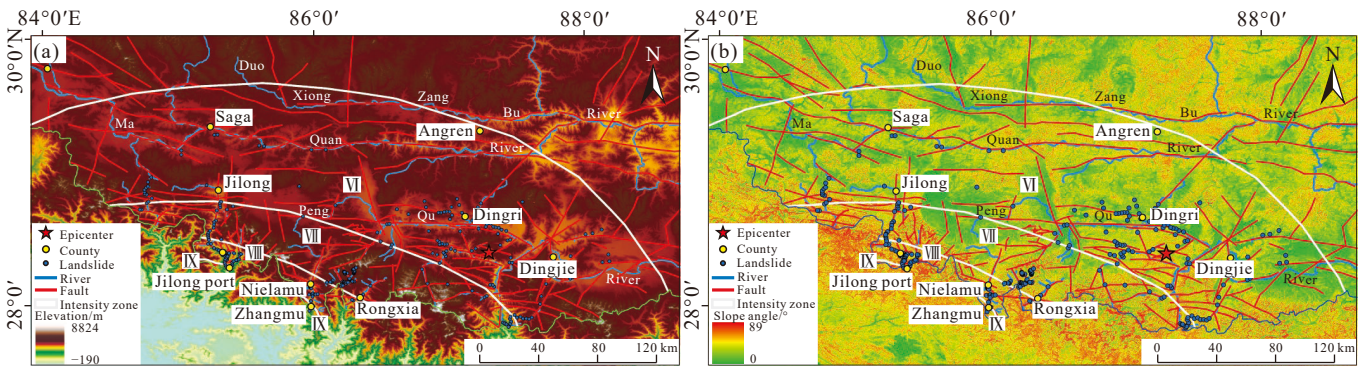

Fig. 7. Relationship between the distribution of secondary geohazards and elevation (a) and slope (b) in Dingri earthquake.

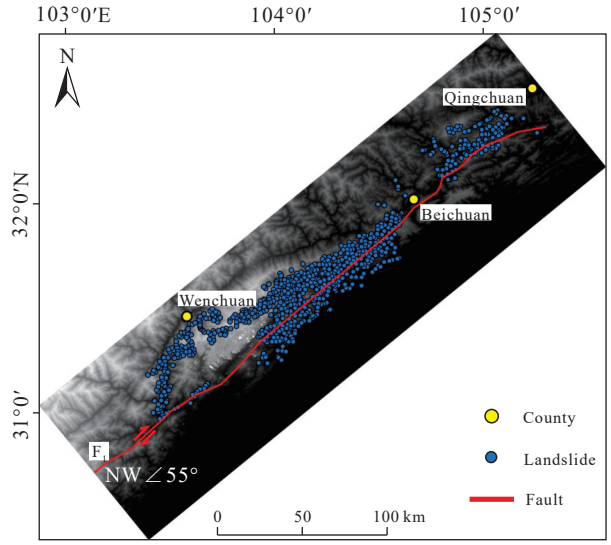

Fig. 8. Comparison of the distribution of geohazard points in the upper/lower wall of the Beichuan-Yingxiu Fault (F_1) in the Wenchuan earthquake.

which objectively reflects the overall vibration intensity around the monitoring stations and provides quantitative information for earthquake damage analysis and assessment. It can be used as first-hand data for rapid prediction, assessment, and zoning of secondary disasters after earthquakes.

In this study, from the PGA data of eight earthquake areas (Table 3), the relationship between the maximum PGA value and the number of secondary geohazards is deciphered (Fig. 9). Due to the remote location of the Yushu and Dingri earthquake areas, when the earthquake occurred, there was no motion observation station far from the epicenter, and therefore, the motion data of the two earthquakes was not collected. Through comparative analysis, the following two points can be obtained:

(i) The maximum seismic PGA is positively correlated with the number of secondary geohazards (R = 0.47). In the three earthquake areas of $PGA_{(max)}$ > 0.9 g (Wenchuan, Lushan and Ludian), several geohazards have appeared, whereas the individual scale and harm always caused were far greater than that in other areas.

Pearson correlation coefficients were calculated according to:

$$R = \frac{n\sum XY - \sum X \sum Y}{\sqrt{n\sum X^2 - (\sum X)^2} \times \sqrt{n\sum Y^2 - (\sum Y)^2}}$$

where R is correlation coefficient, X is the number of secondary geohazards, Y is the maximum seismic PGA, and n are the number of earthquakes.

(ii) The maximum seismic PGA appears in the horizontal direction (EW and NS) and shows that horizontal ground motion plays a leading role in the formation of secondary geohazards, whereas vertical ground motion promotes the formation of secondary geohazards.

5.3. Topographic slope and geomorphic height difference

Usually, under the influence of effective potential energy and high topographic magnification effect, the probability of the occurrence of secondary geohazards is positively correlated with the topographic slope and geomorphic height difference in the earthquake area, the steeper the slope the greater the height difference and the greater the probability of secondary geohazards. However, factors such as lithology, human disturbance, and vegetation coverage should also be considered; when the rock mass is intact, lithology is hard, human engineering activities are low, and vegetation coverage is high, the probability of secondary geohazards in the earthquake area will be reduced. In addition, this study found that the steeper the topographic slope and the greater the geomorphic height difference, the greater the possibility of high-altitude and high-speed remote landslides, and the more serious the harm caused. For example, the Daguangbao landslide with a volume of 1159×10^6 m^3 induced by the Wenchuan earthquake, with a height difference of approximately 1600 m, and a slope of 40°–50°, was the largest landslide ever recorded in China's history (Huang RQ et al., 2014; Cui SH et al., 2020; Liu LJ et al., 2020). The Donghekou landslide in the Wenchuan earthquake, with a volume of > 100×10^6 m^3, a height difference of 700 m, and a slope of 40°–50°, buried 7 villages and killed over 780 people (Yin YP et al., 2016; Song ZC et al., 2018). The Ganjiazhai landslide induced by the Ludian earthquake, with a volume of approximately 1.4×10^6 m^3, a height difference of approximately 800 m, and a slope of 30°–60°, buried the whole village and killed over 50 people (Xu YQ et al., 2016).

Table 3. PGA maximum corresponding station information for nine earthquakes.

NO.	Earthquake name	Station name	Station code	Instrument type	$PGA_{(max)}$/g	Direction	Epicenter distance/km	Site type
1	Wenchuan earthquake	Wolong	051WCW	ETNA	0.98	EW	19	Soil
3	Lushan earthquake	Baoxing	051BXD	MR2002	1.02	EW	9.7	soil
4	Minxian–Zhangxian earthquake	Minxian	062MXT	MR2002	0.18	EW	18	Soil
5	Yiliang earthquake	Yiliang	053YLT	K2	0.1	NS	10.4	Rock
6	Ludian earthquake	Longtoushan	053LLT	ETNA	0.97	EW	4.4	Soil
7	Jinggu earthquake	Yongping	053JYP	ETNA	0.64	NS	6.9	soil
8	Yingjiang earthquake	–	053LHS	K2	0.14	EW	26.5	Soil
9	Dêqên earthquake	Zigeng	–	ETNA	0.43	EW	12.9	Cement

Note: a–Data for this study are provided by China Strong Motion Network Centre at Institute of Engineering Mechanics, China Earthquake Administration. b–dêqên's data obtained from Lai M et al., 2014; c-there was no motion observation station in Yushu and Dingri earthquake areas.

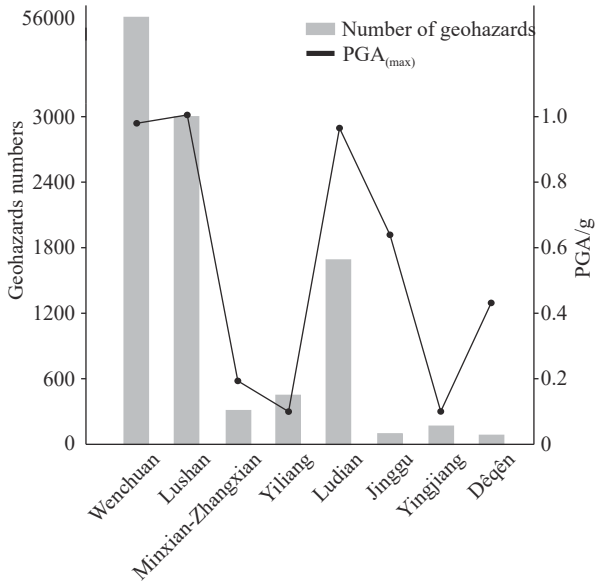

Fig. 9. Relationship between the $PGA_{(max)}$ and the number of secondary geohazards.

By comparing the slope distribution of secondary geohazards induced by the ten earthquakes (Table 4; Fig. 10), the following regimes can be defined:

(i) The greater the geomorphic height difference and the steeper the average slope, the greater the number of geohazard points on the high slope (such as Wenchuan, Dêqên, and Dingri); on the contrary, the smaller the geomorphic height difference and the lower the average slope, the greater the number of geohazard points on low slopes (such as Yingjiang, Jinggu, and Yiliang).

(ii) When the average slope ⩽19°, the disaster points are mainly concentrated between 0°–20°; when the average slope >19°, the disaster points are mainly concentrated between 20°–40°.

(iii) When the topographic slope is <40°, the proportion of secondary geohazards is higher; when the topographic slope is ⩾40°, the proportion of secondary geohazards decreases significantly. Overall, 0°–40° is the prone slope range of earthquake-induced secondary geohazards.

5.4. Distance of fault zone and river system

When an earthquake occurs, the fault zone suddenly rapidly produces substantial dislocation, which destroys the mechanical balance and material structure in the rock mass and forms several fractures in the tensile zone and the compression uplift zone, leading to many secondary geohazards. Meanwhile, the downcutting of the river system and long-term scouring and soaking of the slope foot by water flow not only changes the composition and structure of the rock and soil of the riverbank, but also provides favorable topographic and geomorphic conditions for the occurrence of geohazards. From Figs. 2–7, it can be seen that the secondary geohazards are mainly distributed in the shape of "belt" along the fault and are "linear" along the river system, indicating that the fault zone and river system control the geohazard distribution pattern. According to statistics analysis, 94 large-scale high-speed landslides occurred within the range of 3 km from the seismogenic fault in the Wenchuan earthquake, accounting for more than half of the total number of large landslides regionally (Xu Q, 2010). The closer to the seismogenic fault, the greater the density and scale of the landslide, and there is a negative exponential relationship between the density and the distance from the fault and river system (Huang RQ et al., 2009; Qi SW et al., 2010).

In this study, using the spatial analysis functionality of ArcGIS, the distance from the secondary geohazard points to the seismogenic fault, associated faults and river system in the 10 earthquake areas was extracted. This allowed the relationship between the distribution proportion of geohazard points and the distance to the faults and river system to be examined (Fig. 11). The following regimes can be identified through this comparison:

(i) Fig. 11a shows that, overall, the distribution proportion of secondary geohazards is inversely proportional to the distance to the seismogenic fault. However, large variability is observed in other earthquake areas, whereas the number of disaster points in some earthquake areas was increased even far from the seismogenic fault. In Fig. 11b, the curve of the distance between geohazards and associated faults shows a better correlation, which explains why the number of secondary geohazards was increased despite being far from seismogenic faults.

This shows that the formation of earthquake secondary geohazards is not only related to seismogenic fault but also influenced by the associated faults in the earthquake area.

Table 4. Comparison of slope distribution of secondary geohazards induced by 10 earthquakes in western China since 2008.

No.	Earthquakename	Geomorphic height difference/m	Average slope/°	Percentage of disaster points with different slopes					
				0°–10°	10°–20°	20°–30°	30°–40°	40°–50°	>50°
1	Wenchuanearthquake	7035	20.3	6.2%	14.6%	27.8%	33.4%	13.2%	4.8%
2	Yushuearthquake	3924	18.6	21.6%	23.%	28.1%	20.1%	6.5%	0.7%
3	Lushanearthquake	5522	19.0	28.4%	23.9%	25.6%	17.0%	4.0%	1.1%
4	Minxian-Zhangxianearthquake	4271	19.0	30.4%	39.8%	22.5%	6.1%	0.9%	0.3%
5	Yiliangearthquake	2929	17.9	13.3%	36.1%	32.7%	13.0%	3.4%	1.5%
6	Ludianearthquake	3842	19.5	20.0%	32.4%	25.8%	15.8%	5.6%	0.4%
7	Jingguearthquake	3107	19.1	28.1%	42.7%	28.1%	1.1%	–	–
8	Yingjiangearthquake	3623	15.1	41.9%	37.1%	15.1%	4.8%	1.1%	–
9	Dêqêneearthquake	5362	27.7	10.5%	22.1%	33.7%	20.9%	9.3%	3.5%
10	Dingriearthquake	9014	19.8	17.9%	19.1%	21.8%	23.4%	13.8%	4.0%

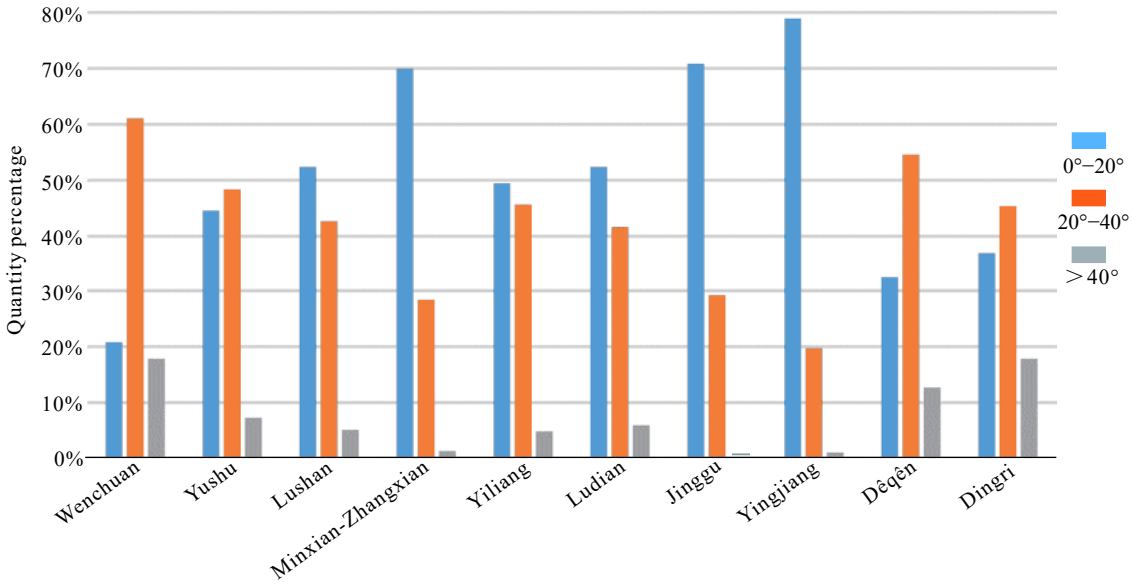

Fig. 10. Relationship between topographic slope and proportion of secondary geohazards.

(ii) It can be seen from Fig. 11c that the distribution of secondary geohazard points is negatively correlated with the distance to the river system, and it is mainly concentrated between 0–6 km from the river system.

(iii) Compared with Figs. 11a–c, it can be found that the curve between the distribution ratio of geohazards and the distance of the river system shows a better response relationship; that is, the fluctuation in the curve is smaller and the changing trend is more stable, indicating that the distribution of disaster points is more evidently affected by the river system, which also follows the actual investigation in the field.

6. Conclusions

Through comparative analysis of the factors influencing the generation of secondary geohazards induced by ten earthquakes, constraints on the main controlling factors were obtained. Such information provides crucial insight into strategies for pre-earthquake disaster prevention and post-earthquake emergency rescue operations, helping to reduce the losses caused by earthquake disasters. The following insights have been obtained from our study:

(i) The occurrence of seismic geohazards is usually affected by many controlling factors, among which the active nature of the seismogenic fault, seismic PGA, topographic slope, and geomorphic height difference in the seismic area, and distance from the fault zone and river system are the most important.

(ii) Compared with strike-slip earthquakes, thrust earthquakes induce more high-altitude and high-speed remote landslides, which are more numerous, cause more serious harm, and have a significant upper/lower wall effect, such as the Wenchuan earthquake on May 12, 2008.

(iii) The slope range 0° –40° is most prone to seismic secondary geohazards; secondary disaster points are mainly concentrated between 0 –6 km from the river system; secondary geohazards are not only related to seismogenic fault but also influenced by the associated faults in the earthquake area.

(iv) The maximum seismic PGA is positively correlated with the number of secondary seismic geohazards, and the horizontal ground motion plays a leading role in the formation of secondary geohazards, whereas the vertical ground motion plays a promoting role.

CRediT authorship contribution statement

Chao Peng and Zhi-qiang Yin conceived of the presented idea. Chao Peng, Zhi-qiang Yin, Hai Shao, and Ming-fei Pang conducted the survey. Xu-jiao Zhang supervised the project. All authors discussed the results and contributed to the final manuscript.

Declaration of competing interest

The authors declare no conflicts of interest.

Acknowledgement

This research was jointly supported by the National Natural Science Foundation of China (41977258), the National Key Research and Development Program of China (2017YFC1501005 and 2018YFC1504704).

Supplementary dataset

The Ministry of Land and Resources of the People ’s Republic of China. 2010. Summary of emergency work for “4.14 ” Yushu earthquake geological disaster in Qinghai Province.

Geo-Environment Monitoring Institute of Gansu Province. 2013. Investigation report on hidden danger of secondary geological hazards in M_S 6.6 earthquake area of Minxian–Zhangxian County, Gansu Province.

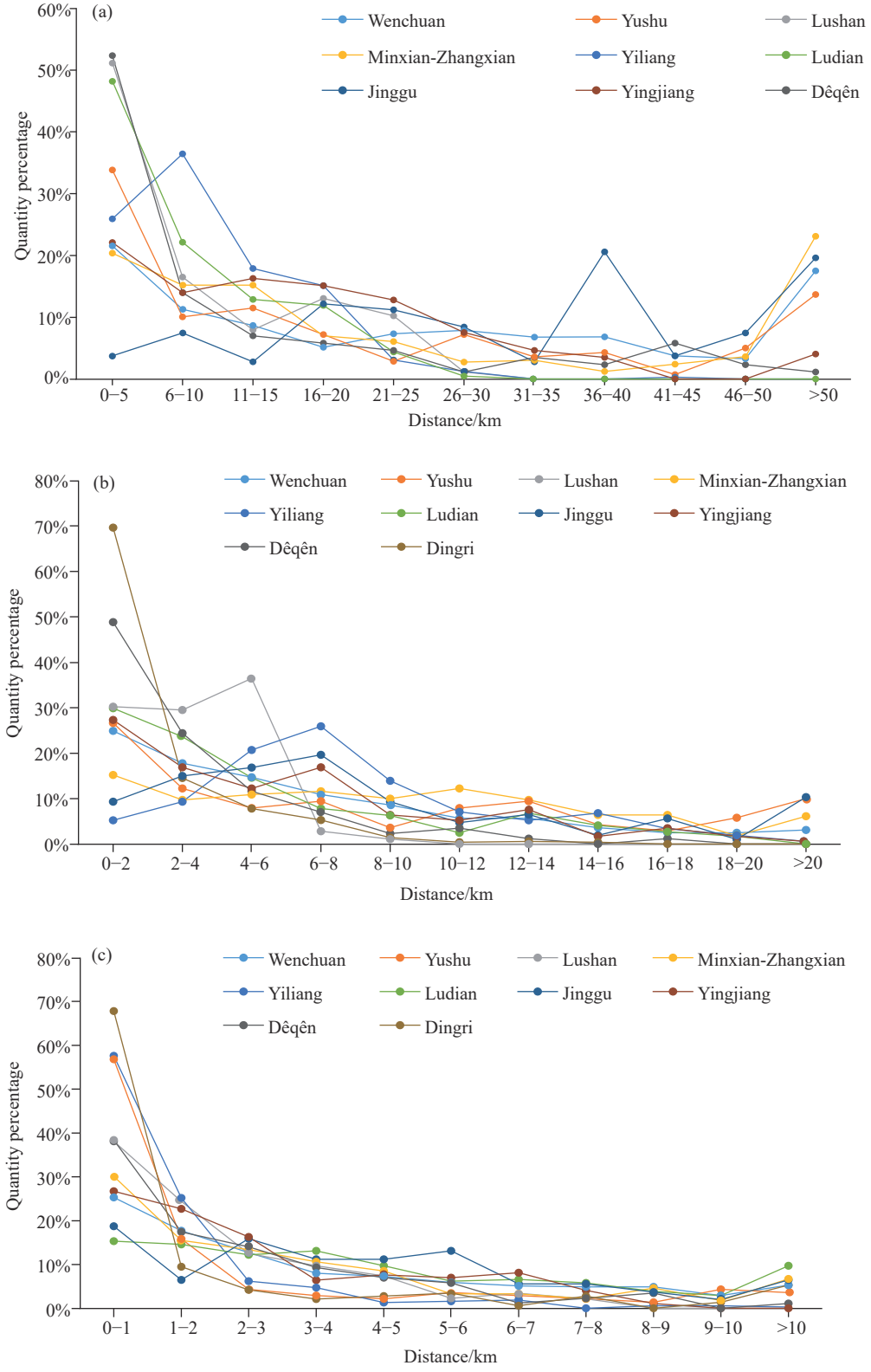

Fig. 11. Curve of the relationship between the distribution ratio of geohazards and its distance to (a) seismogenic fault , (b) associated faults and (c) river system in the earthquake area.

Geo-Environment Monitoring Institute of Yunan Province. 2012. Emergency investigation report of "9.07" earthquake geological disaster in Zhaotong City, Yunnan Province.

Geo-Environment Monitoring Institute of Yunan Province. 2014. Emergency investigation report on hidden danger of geological disaster in "10.7" earthquake disaster area of Jinggu County, Yunnan Province.

Geo-Environment Monitoring Institute of Yunan Province. 2014. Emergency investigation report on "5.24" and "5.30" earthquake geological hazards in Yingjiang County, Dehong Prefecture.

Geo-Environment Monitoring Institute of Yunan Province. Investigation report on hidden dangers of geological disasters after “8.28” and “8.31” earthquake in Diqing Prefecture.

Geological Disaster Emergency Technical Guidance Center of the Ministry of Land and Resources of China. 2015. Work report of the expert group on the emergency response of geological disasters in the “4.25” earthquake disaster area in Tibet.

References

Chen JP, Li JF, Qin XW, Dong QJ, Sun Y. 2009. RS and GIS-based statistical analysis of secondary geological disasters after the 2008 Wenchuan Earthquake. Acta Geologica Sinica (English Edition), 83(4), 776–785. doi: 10.1111/j.1755-6724.2009.00101.x.

Cui P, Zhu YY, Han YS, Chen XQ, Zhuang JQ. 2009. The 12 May Wenchuan earthquake-induced landslide lakes: Distribution and preliminary risk evaluation. Landslides, 6(3), 209–223. doi: 10.1007/s10346-009-0160-9.

Chen XL, Li CY, Wang MM, Li ZF. 2011. The main factors causing the seismic landslide distribution different on two side of the faults–A case of landslide distribution in Beichuan area. Chinese Journal of Geophysics, 54(3), 737–746 (in Chinese with English abstract). doi: 10.3969/j.issn.0001-5733.2011.03.013.

Cui SH, Yang QW, Pei XJ, Huang RQ, Guo B, Zhang WF. 2020. Geological and morphological study of the Daguangbao landslide triggered by the M_S 8.0 Wenchuan earthquake, China. Geomorphology, 370, 107394. doi:10.1016/j.geomorph.2020.107394

Ding YH, Wang YQ, Sun JZ. 1999. Correlation between seismic landslide and collapse and seismic parameters and its application in predicting slope earthquake disaster. Chinese Journal of Geophysics, 42(S1), 101–107 (in Chinese with English abstract). doi: 10.1016/S0009-2541(98)00159-4.

Dai FC, Xu C, Yao X, Xu L, Tu XB, Gong QM. 2011. Spatial distribution of landslides triggered by the 2008 M_S 8.0 Wenchuan earthquake, China. Journal of Asian Earth Sciences, 40(4), 883–895. doi:10.1016/j.jseaes.2010.04.010

Huang RQ, Li WL. 2009. Fault effect analysis of geo-hazard triggered by Wenchuan earthquake. Journal of Engineering Geology, 17(1), 19–28 (in Chinese with English abstract). doi: 10.3969/j.issn.1004-9665.2009.01.003.

Huang RQ, Zhang WF, Pei XJ. 2014. Engineering geological study on Daguangbao landslide. Journal of Engineering Geology, 22(4), 557–585 (in Chinese with English abstract). doi: 10.13544/j.cnki.jeg.2014.04.004.

Han YS, Liang C, Cui P, Han J, Xue J, Zhang YX. 2010. Susceptibility of mountain hazards triggered by Wenchuan earthquake to topographic factors. Journal of Sichuan University (Engineering Science Edition), 42(S1), 15–21 (in Chinese with English abstract). doi: 10.15961/j.jsuese.2010.s1.001.

Li XJ, Zhou ZH, Huang M, Wen RZ, Yu HY, Lu DW, Zhou YN, Cui JW. 2008. Preliminary analysis of strong-motion recordings from the magnitude 8.0 Wenchuan, China, Earthquake of 12 May 2008. Seismological Research Letters, 79(6), 844–854. doi: 10.1785/gssrl.79.6.844.

Lai M, Zhu JG, Jiang P, Sun ZT, Li DH, Yu H, Long CH, Zhu YL. 2014. Ground motion data study of the 2013 Dêqên-Derong M_S 5.9 Earthquake. Earthquake Research in Sichuan, (1), 5–8 (in Chinese with English abstract). doi: 10.13716/j.cnki.1001-8115.2014.01.002.

Liu CZ, Wen MS, Liu YH, Liu QQ, Gu XX. 2016. Regional assessment on geological disasters in “5.12” Wenchuan seismic area, China. Hydrogeology and Engineering Geology, 43(5), 1–16 (in Chinese with English abstract). doi: 10.16030/j.cnki.issn.1000-3665.2016.05.01.

Liu LJ, Fu HY, Zhang YB, Wang JM, Wang QD, Xiang CL, Cheng QG. 2020. DDA simulation of the mobility of Daguangbao landslide considering the frictional weakening of sliding bed. Journal of Engineering Geology, 28(6), 1221–1232 (in Chinese with English abstract). doi: 10.13544/j.cnki.jeg.2019-307.

Lan J, Chen XL. 2020. Evolution characteristics of landslides triggered by 2008 M_S 8. 0 Wenchuan earthquake in Yingxiu area. Seismology and Geology, 42(1), 125–146 (in Chinese with English abstract).

Qi SW, Xu Q, Lan HX, Zhang B, Liu JY. 2011. Spatial distribution analysis of landslides triggered by May 12 2008 Wenchuan Earthquake, China. Engineering Geology, 116(1-2), 95–108. doi: 10.1016/j.enggeo.2010.07.011.

Song ZC, Zhao LH, Li L, Zhang YB, Tang GP. 2018. Distinct element modelling of a landslide triggered by the May 12 Wenchuan earthquake: A case study. Geotechnical and Geological Engineering, 36(4), 2533–2551. doi: 10.1007/s10706-018-0481-3.

Tang C, Zhu J, Qi X, Ding J. 2011. Landslides induced by the Wenchuan earthquake and the subsequent strong rainfall event: A case study in the Beichuan area of China. Engineering Geology, 122(1–2), 22–33. doi: 10.1016/j.enggeo.2011.03.013.

Wang XY, Nie GZ, Wang DW. 2010. Research on relationship between landslides and peak ground acceleration induced by Wenchuan earthquake. Chinese Journal of Rock Mechanics and Engineering, 29(1), 82–89 (in Chinese with English abstract).

Wang XY. 2010. Study of fast evaluation technique of earthquake-induced landslides and their effects on earthquake emergency rescue. Chinese Journal of Rock Mechanics and Engineering, 29(10), 2159 (in Chinese with English abstract).

Wang XY, Wang DW. 2011. Relationships between the Wenchuan earthquake -induced landslide and peak ground velocity, Sichuan, China. Geological Bulletin of China, 30(1), 159–165 (in Chinese with English abstract). doi: 10.3969/j.issn.1671-2552.2011.01.017.

Wang YF, Cheng QG, Zhu Q. 2012. Inverse grading analysis of deposit from rock avalanches triggered by Wenchuan earthquake. Chinese Journal of Rock Mechanics and Engineering, 31(6), 1089–1106 (in Chinese with English abstract). doi: 10.3969/j.issn.1000-6915.2012.06.002.

Wang DP, He SM, Ge SJ, Pan CP, Zhai MG. 2013. Mountain hazards induced by the earthquake of Sep 07, 2012 in Yiliang and the suggestions of disaster reduction. Journal of Mountain Science, 31(1), 101–107 (in Chinese with English abstract). doi: 10.3969/j.issn.1008-2786.2013.01.014.

Wang Y, Yang YD, Yan XS, Tang P, Zhang, J. 2016. Characteristics and causes of super-huge secondary geological hazards induced by M_s 6.5 Ludian earthquake in Yunnan. Journal of Catastrophology, 31(1), 83–86 (in Chinese with English abstract). doi: 10.3969/j.issn.1000-811X.2016.01.017.

Wu XN, Yi JM, Zhou SL, Yin ZQ, Xu YQ. 2017. A study on the active faults structures and geohazards triggered by the M_S 8.1 earthquake in Nepal. Hydrogeology and Engineering Geology, 44(4), 137–144 (in Chinese with English abstract). doi: 10.16030/j.cnki.issn.1000-3665.2017.04.21.

Wu WY, Xu C, Wang XQ, Tian YY, Deng F. 2020. Landslides triggered by the 3 August 2014 Ludian (China) Mw 6.2 Earthquake: An updated inventory and analysis of their spatial Distribution. Journal of Earth Science, 31(4), 853–866. doi: 10.1007/s12583-020-1297-7.

Xu Q. 2010. Study on Large-scale Landslides in Wenchuan Earthquake. Beijing, Science Press, 1–12 (in Chinese).

Xu C, Xu XW, Yu G. H. 2012. Study on the characteristics, mechanism, and spatial distribution of Yushu earthquake trigged landslides. Seismology and Geology, 34(1), 47–62 (in Chinese with English abstract). doi: 10.3969/j.issn.0253-4967.2012.01.006.

Xu YQ, Yin ZQ, Sa LP. 2016. Developing characteristics and evolution

process of Ganjiazhai large scale landslide in Ludian 3rd August earthquake area of northeast Yunnan. Journal of Engineering Geology, 24(4), 550–558 (in Chinese with English abstract). doi: 10.13544/j.cnki.jeg.2016.04.009.

Xiao WB, Chen YY, Wang YB, Zhang YS. 2020. Reginal seismic wave propagation modeling and ground motion characteristics of the 2013 M_S 3rd August Minxian earthquake in Gansu. Chinese Journal of Geophysics, 63(5), 1816–1829 (in Chinese with English abstract). doi: 10.6038/cjg2020N0373.

Yuan RM, Tan XB, Chen GH, Xu XW. 2010. Huge landslides occurred at the special places of the coseismic rupture and their mechanism explanation based on the formation model of tectonic-geomorphology: A case study of Donghekou ejection landslide. Earth Science Frontiers, 17(5), 243–253 (in Chinese with English abstract). doi: 10.1017/S0004972710001772.

Yin YP, Zheng WM, Li XC, Sun P, Li B. 2011. Catastrophic landslides associated with the M_S 8.0 Wenchuan earthquake. Bulletin of Engineering Geology and the Environment, 70(1), 15–32. doi: 10.1007/s10064-010-0334-7.

Yin YP, Zhang YS. 2012a. Wenchuan earthquake engineering geology and geological disaster. Beijing, Science Press, 375 –385 (in Chinese).

Yin YP, Wang M, Li b, Feng Z. 2012b. Dynamic response characteristics of Daguangbao landslide triggered by Wenchuan earthquake. Chinese Journal of Rock Mechanics and Engineering, 31(10), 1969–1982 (in Chinese with English abstract). doi: 10.3969/j.issn.1000-6915.2012.10.003.

Yang J, Zeng ZX, Li MH, Fang YG, Tan ZS, Wu SZ, Gong, C. 2015. The seismo-geological hazards and seismogenic structure of the 2013 Dêqêng-Derong 5.9 earthquake. Earth Science-Journal of China University of Geosciences, 40(10), 1701–1709 (in Chinese with English abstract). doi: 10.3799/dqkx.2015.153.

Yin YP, Wang WP, Li B, Zhang N, Li HT. 2016. Study of stratigraphic site effect on the failure mechanism of Donghekou rockslide triggered by Wenchuan earthquake. China Civil Engineering Journal, 49(S2), 126–131 (in Chinese with English abstract). doi: 10.15951/j.tmgcxb.2016.s2.022.

Yin ZQ, Xu YQ, Chen HQ, Sa LP, Jiang XW. 2016. The development and distribution characteristics of geohazards induced by August 3, 2014 Ludian earthquake and comparison with Jinggu and Yingjiang earthquake. Acta Geologica Sinica, 90(6), 1086–1097 (in Chinese with English abstract). doi: 10.3969/j.issn.0001-5717.2016.06.003.

Yin ZQ, Zhao WJ, Xu YQ, Sa LP. 2017. Distribution characteristics of geohazards induced by the Ludian earthquake on 3 August, 2014 and a comparison to the Jinggu and Yingjiang earthquakes. Advancing Culture of Living with Landslides, 4, 95–110. doi: 10.1007/978-3-319-53485-5_11.

Yang XY, Yao YH. 2018. Development law and distribution characteristics of geological hazards after “8.03 ” earthquake in Ludian, Yunnan Province. China Earthquake Engineering Journal, 40(5), 1078–1083 (in Chinese with English abstract). doi: 10.3969/j.issn.1000-0844.2018.05.1078.

Zhou BG, Zhang YM. 1994. Some characteristics of earthquake induced landslide in Southwestern China. Northwestern Seismological Journal, 16(1), 95–103 (in Chinese with English abstract).

Zhang YS, Dong SW, Hou CT, Guo CB, Yao X, Li B, Du JJ, Zhang JG. 2013. Geohazards induced by the Lushan M_S 7.0 Earthquake in Sichuan Province, Southwest China: Typical examples, types and distributional characteristics. Acta Geologica Sinica (English Edition), 87(3), 646–657. doi: 10.1111/1755-6724.12076.